Protocol

A new method for imaging and 3D reconstruction of mammalian cochlea by fluorescent confocal microscopy

Natalie A. Hardie[1], Glen MacDonald[1], Edwin W Rubel*

Virginia Merrill Bloedel Hearing Research Center and Otolaryngology-HNS, University of Washington, Box 357923, Seattle, WA 98195-7923, USA

Abstract

Traditional methods for anatomical and morphometric studies of cochlear tissues have relied upon either microdissection of the organ of Corti or the generation of serial sections of the cochlea. Such methods are time-consuming, disruptive to three-dimensional relationships and often restrict sampling to very limited numbers of cells. We have found that cells and tissue components of the cochlear duct may be labelled by fluorescent markers within intact cochleae, which are then embedded in epoxy resin for subsequent viewing by fluorescent microscopy methods. This approach allows imaging through thick optical volumes with preservation of three-dimensional relationships. Unlike sectioned tissue, alignment of the sample relative to the focal axis may be easily corrected by re-orientation of the optical volume with common image processing software. Fluorescently labelled cochleae embedded in epoxy can be viewed by most fluorescent microscopy methods including laser scanning confocal microscopy, multi-photon confocal microscopy and widefield epi-fluorescence microscopy with deconvolution. Furthermore, semi-thin sections made from these preparations are compatible with traditional histological stains, as well as allowing brightly labelled epi-fluorescent images.
© 2004 Elsevier B.V. All rights reserved.

1. Introduction

The cochlea is a complex structure, consisting of relatively large fluid-filled spaces and a wide variety of tissue types ranging from acellular gelatinous material (the tectorial membrane) and dense bone (the otic capsule) to the remarkably delicate hair cells. These structures are arranged in a complex, helical geometry spiralling around a central pillar of spongy bone, the modiolus (Figs. 1A and 2C). Traditional methods of microscopic examination of the cochlea require either microdissection of the organ of Corti [2], or the generation of sections from plastic or paraffin-embedded tissue. However, the geometry of the cochlea makes precise tissue orientation for histological processing and viewing technically challenging. The three-dimensional relationships between cochlear structures or cell types are often difficult to

determine using traditional, two-dimensional sections, requiring tedious serial sectioning and reconstruction [4–6]. In addition, many embedding materials can result in the loss of tissue antigenicity, making it difficult to perform immunochemical studies on sectioned material. Frozen sections preserve most tissue antigenicity and can provide thicker sections that do allow some depth of field. However, the advantages of frozen sections are often at the expense of the microscopic integrity of the more delicate cochlear tissues. Some of these issues have been partly overcome by imaging the cochlea in vitro with laser scanning confocal microscopy, after application of fluorescent vital labels [3].

Some strains of mice undergo an age-related sensorineural hearing loss, comparable to presbycusis in humans. Presbycusis is a degenerative process typically involving loss of outer hair cells (OHCs) followed by collapse of the organ of Corti and loss of the inner hair cells (IHCs). This pattern of degeneration generally begins in the basal (high frequency) turn of the cochlear duct and progresses toward the apical (low frequency) turn. Our research required comparisons of IHC number and innervation in apical and basal

---

* Corresponding author. Tel.: +1-206-543-8360; fax: +1-206-221-5685.
E-mail address: rubel@u.washington.edu (E.W Rubel).
[1] These two authors contributed equally to this work.
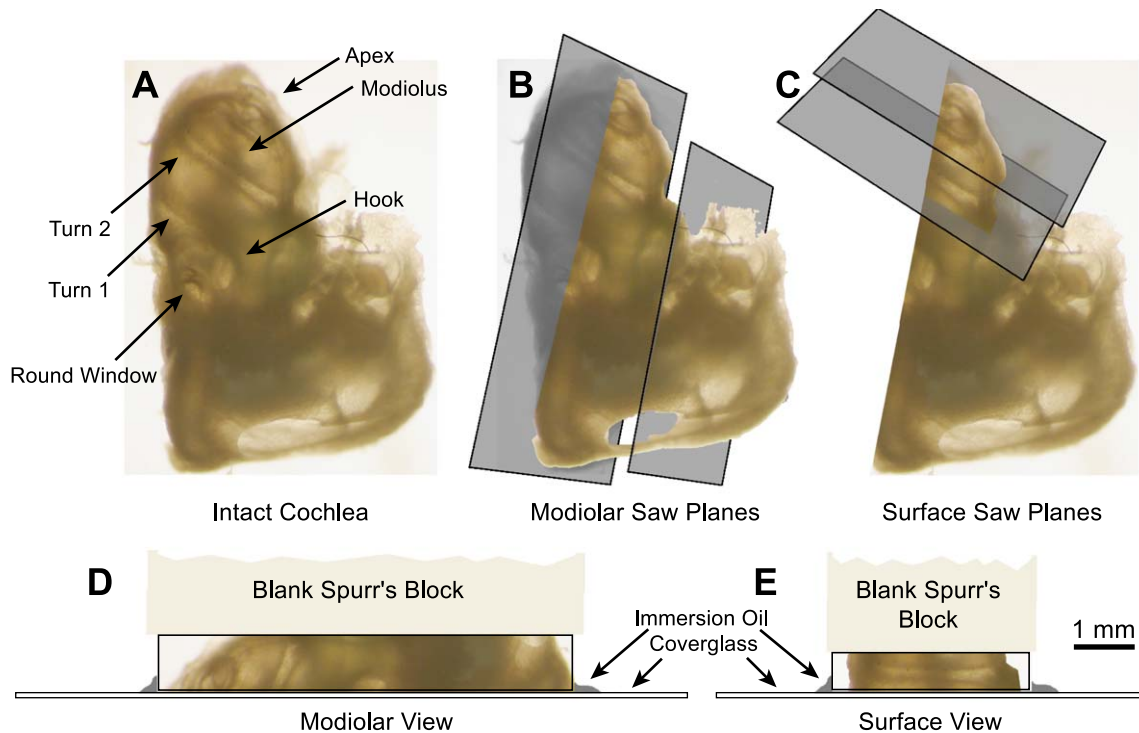
Fig. 1. Preparation of modiolar view and surface view samples is illustrated using an intact cochlea from a CBA mouse, postnatal day 7, viewed with backlighting. (A) The apex and dorsal edge of the round window are aligned with the modiolar axis. The modiolus, lower (T1) and upper (T2) turns may be seen through the thin otic capsule, as may the hook region of the organ of Corti curving around the round window. (B) The larger gray panel represents the plane in which the cochlea is bisected; the smaller gray panel is the parallel plane in which extraneous bony material and plastic is removed for a modiolar view. (C) The hemisected cochlea is sawn in planes perpendicular to the modiolar plane to create surface views; the upper turn is being removed in this example. (D) An illustration of a hemisected cochlea positioned on a coverglass in a modiolar view as described in Section 5.5. (E) A cochlear turn prepared for a surface view is illustrated, as described in Section 5.5.

turns between mouse strains with varying susceptibilities to presbycusis.

We describe a new, efficient method for using confocal microscopy for morphometry and three-dimensional imaging of the cochlea following immunohistochemistry and plastic embedding. The 3D nature of this approach allows specifically labelled cells to be imaged and counted along a portion of the cochlear duct, and enables morphometric analyses not possible using either cultured sensory epithelium or serial tissue sections. The tissue remains suited to subsequent sectioning into semi-thin sections for traditional light microscopic analysis, if desired.

The technique of embedding tissue in epoxy resin following immunohistochemistry has been previously applied to combined confocal and transmission electron microscopy studies of the nervous system of the moth, *Manduca sexta* [8]. We believe our report is the first using this approach in the cochlea.

2. Type of research

- Morphometric analysis of cochlear tissues
- High-resolution microscopy of cochlear anatomy and functional relationships

- Three-dimensional reconstructions and morphometry for peripheral and central neuroanatomy.

3. Time required

The dissection, fixation, immunhistochemical labelling and plastic embedding procedures require 10–11 days to complete. If decalcification of the cochlea is required (e.g. for subsequent sectioning of rat or mouse cochlea older than postnatal day 5 (P5)), add 1–7 days of decalcification time, depending on the age of the animal. Confocal scanning requires just a few minutes to generate an optical volume. Time required for subsequent image processing and analysis will vary according to the nature of the analysis.

4. Materials

4.1. Animals

- Postnatal mice of ages from 21 days to 15 months and of several strains (C57BL/6J, 129/C57BL6, Swiss-Webster, CBA) were used in this protocol, but the

essentials of the method should work on any mammal. A total of 56 cochleae from 64 mice were imaged in the course of this work. Mice were either obtained from Jackson Laboratories or from breeding pairs originally obtained from Jackson Laboratories. Animals were euthanized in a carbon dioxide chamber and subsequently decapitated. All procedures were approved by the Institutional Animal Care and Use Committee of the University of Washington School of Medicine.

4.2. Special equipment

- Dissecting microscope (such as a Leica MZ8)
- Microdissecting instruments including Dumont #5 forceps, scalpel, scissors
- Petri dishes
- Glass vials (screw top, 4 ml, such as those made by VWR International)
- Two Nutators (Clay Adams brand, model #421105, made by TCS Scientific): one at 4 °C, one at room temperature
- Fume hood
- Vacuum desiccator
- Silastic rubber molds for plastic embedding (Pelco 10505)
- Incubator oven set to 60 °C
- Diamond wheel saw (South Bay Technology, model 650)
- Confocal microscope.

4.3. Chemicals and reagents

- 16% paraformaldehyde (Electron Microscopy Sciences, cat. #15710)
- 0.1 M phosphate-buffered saline (PBS), pH 7.2–7.4
- EDTA, reagent grade
- Spurr's Low Viscosity Embedding Media (Electron Microscopy Sciences, cat. #14300)
- Propylene oxide.

4.4. Tissue labelling reagents

- Mouse monoclonal anti-calretinin (Chemicon, Temecula, CA)
- Rabbit polyclonal anti-calretinin (Chemicon)
- Mouse monoclonal anti-beta-actin (Sigma, St. Louis, MO)
- Mouse monoclonal anti-Tubulin (Sigma)
- Rabbit polyclonal anti-200 kDa Neurofilament (Chemicon)
- Goat anti-mouse IgG-Alexa 488 (Molecular Probes, Eugene, OR)
- Goat anti-rabbit IgG-Alexa 488 (Molecular Probes)
- Goat anti-mouse IgG-Alexa 594 (Molecular Probes)
- Goat anti-rabbit IgG-Alexa 594 (Molecular Probes)
- Donkey anti-mouse IgG-Cy5 (Jackson ImmunoResearch, West Grove, PA)
- Yo-Pro-1, (DNA label, Molecular Probes)
- To-Pro-3, (DNA label, Molecular Probes)
- Neurotrace Red (RNA label, Molecular Probes).

5. Detailed procedure

5.1. Dissection, fixation and decalcification

Post-fixation, washes and decalcification were carried out with gentle rotation on a Nutator, unless otherwise noted.

1. Prepare fixative: 4% paraformaldehyde in 0.1 M PBS, pH 7.2–7.4 (4% PFA).
2. Obtain cochleas by rapid dissection. Open the skull and remove the brain to expose the underlying temporal bones. Dissect the cochlea and vestibular apparatus away from the surrounding temporal bones and transfer to a Petri dish containing fixative. The entire dissection procedure should take no longer than 1–2 min.
3. Under a dissecting microscope, gently remove the stapes using the point of a number 11 scalpel blade. Carefully incise the round window membrane using a 30-gauge needle. Make a small hole in the apex of the cochlea using the point of a scalpel blade or needle to further enhance solution penetration through the labyrinth. Generate a gentle flow of fixative over the outside of the cochlear capsule to dislodge any air bubbles trapped within the round or oval window opening. Immerse the cochlea in fresh 4% PFA and post-fix overnight at 4 °C.
4. Wash 3×10 min in 0.1 M PBS at room temperature.
5. If necessary, decalcify by placing in a solution of 10% EDTA in PBS at 4 °C. Change EDTA solution daily until decalcified (test by gently pressing on cochlea with forceps under dissecting microscope).
6. Wash 3×10 min in 0.1 M PBS at room temperature.

5.2. Immunohistochemistry

All incubation and wash steps were carried out with gentle rotation on a Nutator, unless otherwise noted.

1. Wash in 0.1 M PBS+0.1% Triton X-100 for 10 min at room temperature.
2. Incubate in blocking solution (0.5% BSA, 10% normal goat serum, 0.1% Triton X-100 in 0.1 M PBS) for 2 h at 4 °C.
3. Apply primary antibody in blocking buffer and incubate for 3 days at 4 °C. Two primary antibodies (i.e. one monoclonal and one polyclonal) may be applied simultaneously, e.g. rabbit-anti-calretinin and mouse-anti-tubulin, both used at a dilution of 1:500.
4. Wash 3×10 min in 0.1 M PBS, then in 0.1 M PBS+0.1% Triton X-100 for 10 min at room temperature.

5. Apply fluorescent secondary antibody in blocking buffer and incubate for 2 days at 4 °C. Two secondary antibodies directed to primary antibodies derived from different species may be applied simultaneously, e.g. goat-anti-mouse Alexa 488 and goat-anti-rabbit Alexa 594, both at a dilution of 1:500. Secondary antibodies conjugated to the Alexa fluorophores were centrifuged at 10,000 rpm for 10 min, at 4 °C, prior to removing aliquots for working dilutions. Wrap the glass vials in aluminium foil or otherwise protect them from light exposure during subsequent steps.

6. Wash 3×10 min in 0.1 M PBS, then in 0.1 M PBS+0.1% Triton X-100 for 10 min at room temperature.

7. Apply a 2 μM solution of fluorescent DNA stain such as To-Pro-3 or Yo-Pro-1, chosen such that the emission spectra does not overlap with that of the secondary antibodies, in PBS for 45 min at room temperature.

8. Wash 3×10 min in 0.1 M PBS at room temperature.

9. Proceed to dehydration and embedding. Note that osmication of the tissue following immunofluorescent labelling destroys the fluorescence of the secondary antibodies, and is therefore not compatible with this technique.

5.3. Dehydration and infiltration

(1) Prepare the Spurr's resin according to the following recipe: 10 g ERL 4206, 7.6 g DER 736, 26.0 g NSA and 75 μl DMAE. This recipe uses only 1/4 of the usual proportion of the polymerizing agent DMAE, and thus takes a relatively long time to harden.

The following steps are performed at room temperature in a fume hood, with gentle agitation and protected from light.

(2) Dehydrate through graded ethanol solutions: 35%, 70%, 95%, 100%, 100% for 15 min each.

(3) Wash 2×10 min in propylene oxide.

(4) Wash in a 1:1 solution of propylene oxide and freshly made Spurr's resin for 2 h.

(5) Place in 100% Spurr's resin for 1 hour in a vacuum desiccator.

(6) Place in fresh 100% Spurr's resin overnight.

5.4. Embedding

Place cochlea in a silastic mold filled with freshly prepared resin. Orient cochlea so that the round and oval windows are facing upward and the modiolus is parallel to the side wall of the mold. Polymerise at 60 °C for 3–4 days.

5.5. Sectioning

Examine the polymerized cochlea under the dissecting microscope, and use a scalpel blade to make a score line parallel to the modiolus from the apex to the round window (refer to Fig. 1A). Using the diamond wheel saw, hemisect the cochlea by sawing along the score line and along two parallel lines 1 mm to either side of the central cut (Fig. 1B). This creates two 1 mm thick slabs, each containing the half-turns of one side of the cochlea. Attach these slabs to a blank block of Spurr's resin using cyanoacrylate adhesive, with the modiolar surface facing up, and allow to harden. Clean this surface with compressed air and carefully place face down into a small drop of immersion oil on a clean coverslip of 1.5 thickness as shown in Fig. 1D (see Section 5.6). This orientation and view is referred to in the results as a **modiolar view**.

Alternatively, the various cochlear turns may be dissected out of the initial 1 mm slab by sawing between them, parallel to the cochlear duct (Fig. 1C). Portions of the basilar membrane may be viewed as a surface preparation in the manner described previously [1,7]. These smaller pieces may then be glued to a blank Spurr's block for stability and placed on a 1.5 thickness coverslip as described above (Fig. 1E). This orientation and view is referred to in the results as a **surface view**.

5.6. Imaging

Imaging may be performed on a laser scanning confocal microscope (LSCM) system, multiphoton LSCM or by deconvolution of epi-fluorescent images. We used inverted microscopes, which allow the mounted samples to be positioned over the objective lens.

5.6.1. Laser scanning confocal microscopy (LSCM)

We used an MRC-1024UV LSCM (Bio-Rad Laboratories, Hercules, CA) attached to a Nikon Diaphot 300 inverted microscope (Nikon, Melville, NY) to collect a series of images at successive magnifications. This system was equipped with an argon ion laser (Coherent, Santa Clara, CA) and a krypton/argon laser (ILT, Frindley, MN). These two lasers provided excitation lines at 351, 357, 363, 488, 514, 568 and 647 nm. Low power objectives allowed a survey of tissue and orientation for subsequent high magnification images. Z-series stacks were collected with magnification and focus step selected such that the smallest object to be resolved was sampled over at least two pixels at the detector. The effective depth of focus depended upon the objective and desired sample size. A focal depth of 60 μm was used with a $60 \times$ PlanApo objective, NA 1.4 (Nikon), as a compromise between the extent of imaged volume and attenuation of signal through the sample. Red fluorescence was collected in PMT1 with the 605DF32 band-pass filter, green fluorescence was collected in PMT2 with the 522DF35 band-pass filter and far red fluorescence was collected in PMT3 with the 680DF40 band-pass filter while using the T1 and E2 dichroic filter sets.

5.6.2. Multi-photon LSCM

A Zeiss LSM-510MP with a Zeiss Axiovert 200 M (Carl Zeiss Microimaging, Thornwood, NY) allowed two-photon

microscopy of embedded cochlea samples, mounted as described above. Excitation at 810 nm from a Mira tuneable laser pumped by a 5 W Verdi laser (Coherent) allowed simultaneous imaging of Alexa 488 and Alexa 594. The fluorescent emissions were collected in Channel 2 with a 500–530 nm barrier filter and in Channel 1 with a 530LP dichroic.

5.6.3. Deconvolution epi-fluorescent microscopy

Epi-fluorescent imaging was performed with a Marianas imaging system (Intelligent Imaging Innovations, Denver, CO) consisting of a Zeiss Axiovert 200 M coupled by a liquid light guide to a 175 W xenon lamp (Sutter Instrument, Novato, CA) and controlled by Slidebook software. Excitation and emission wavelengths were selected by separate filterwheels and a four-channel dichroic mirror (86000 Sedat Quad Filter, Chroma Technologies, Brattleboro, VT). Green fluorescence excitation: 490/20 nm, emission: 528/38 nm; red fluorescence excitation: 555/28 nm, emission: 617/73 nm; far red fluorescence excitation: 635/20 nm, emission: 685/40 nm.

5.7. Subsequent sectioning

Once confocal images are obtained, the tissue may be sectioned on a conventional microtome to obtain traditional semi-thin plastic sections of the cochlea. The plastic used in this protocol yields good quality sections, which may be examined under a standard fluorescence microscope for detailed localization of immunolabel, or stained with toluidine blue for standard light microscopy.

5.8. Image processing

The optical volumes created by this procedure may be re-oriented in a variety of software applications to enable the
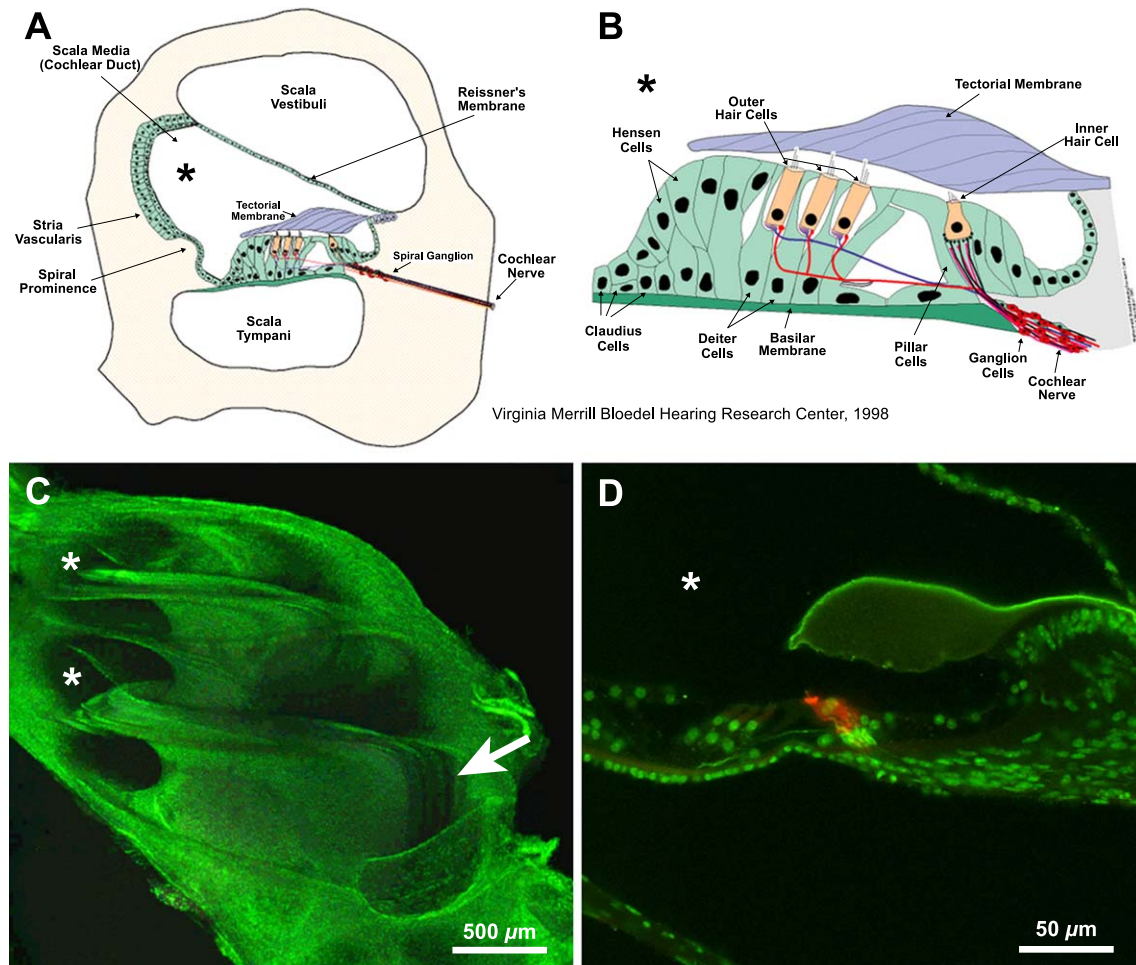
Fig. 2. The organization of the mammalian cochlea is very complex and difficult to appreciate when viewed in thin sections. (A) The organ of Corti (OC) lies in the cochlear duct, surrounded by the bony labyrinth and otic capsule (yellow shading). (B) The three outer hair cells are surrounded by intercellular spaces, while the inner hair cell is embedded in support cells. (C) The side of this otic capsule was sawn away and presents the OC spiralling along the modiolus, with the hook region plunging downwards at the lower right (arrow). This image represents combined autofluorescence and the green DNA label Yo-Pro-1. LSCM , 4× PlanE, NA 0.1 (Nikon). (D) A mid-modiolar section showing the OC in cross section, with the IHC specifically labelled for calretinin (red). The nuclei and neural processes immunolabeled for neurofilament are shown as green. The tectorial membrane is outlined by autofluorescence and nonspecific binding of the secondary antibodies. LSCM, 20× Fluor, NA 0.5 (Nikon). Asterisks mark the scala media in all panels.

sample volumes to be viewed in multiple orientations or to create standardized views. Cell counts and measurements of cell spacings were made using Object Image, an image analysis program in the public domain and freely available from http://simon.bio.uva.nl. The image stacks were opened in Object Image and then three-dimensional objects defined to allow measurements of, for example, the length of the basilar lamina, the distance between IHCs and the number of IHCs through the volume. Following minimal image processing and perhaps re-orientation of the stack into a more favorable orientation, single channel images can be exported as Quicktime movies.

Stacks from multiply labelled samples may be combined in ImageJ, freely available from http://rsb.info.nih.gov/ij/ to create rotating projections in 24-bit color to demonstrate a 3D view of the sample. These may also be exported as Quicktime movies.

Iso-surface renderings can be created in various software packages to allow rotating 3D images to be viewed in standardized orientations. Voxblast (Vaytek, Fairfield, IA)

allowed surface rendering with arbitrary re-orientation into standard views. The Voxblast palette tool was extremely useful in separating broad-spectrum autofluorescence collected in multiple detector channels from specific nuclear labels. We also used Slidebook to produce interactive Quicktime VR 3D models.

Deconvolution was applied to optical volumes collected by both LSCM and multi-photon microscopy. Nearest neighbor and constrained iterative algorithms were applied using Slidebook.

6. Results

The Spurr's resin did not demonstrate significant inherent fluorescence at routine LSCM detector settings, even upon excitation at 351 or 363 nm from an Argon ion laser, with power levels up to 10 mW, measured at the back focal plane of the objective. The concentration of the epoxy resin hardening accelerator, DMAE, was reduced in an attempt
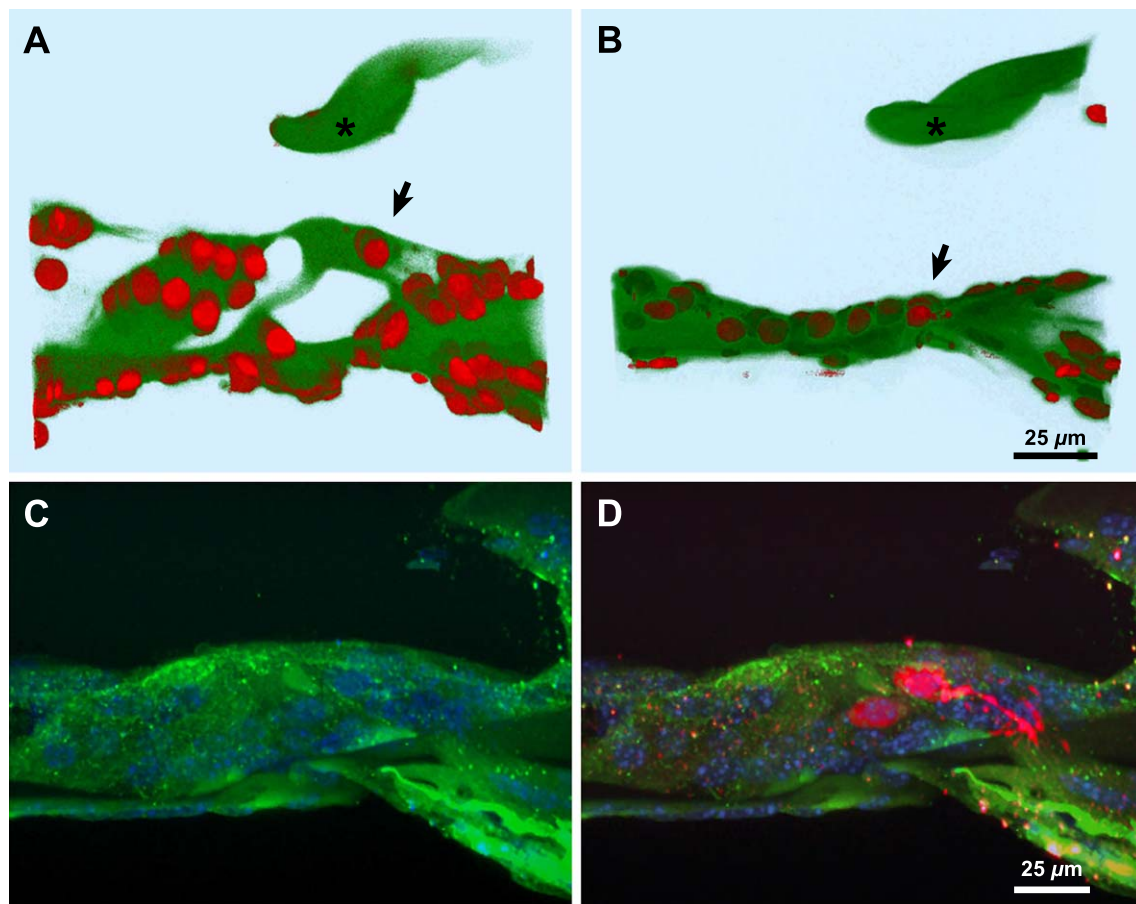
Fig. 3. Cell recognition in a degenerating OC is very difficult without cell-specific markers. (A, B) Isosurface reconstructions of normal and degenerated organs using autofluorescence (green) and Yo-Pro-1 DNA label (red) provide modiolar views arbitrarily rotated to present cross sections of the cochlear duct. (A) The organ from a 2-month-old C57BL/6J mouse displays normal organization and clearly recognizable IHC nuclei (arrow). (B) A 15-month-old C57BL/6J mouse OC shows signs of severe degeneration and nuclei suggestive of IHC (arrow), but it is difficult to identify cell types. (C) IHC nuclei cannot be distinguished in a brightest point projection from a 12-month-old C57BL/6J mouse labelled for beta-actin (green), nuclei (blue) and calretinin (not shown). (D) The same image as panel 3C, but the IHCs are now clearly identified by adding the calretinin label (red). LSCM, 60× PlanApo objective, NA 1.4 (Nikon).

to prevent potential oxidative damage to the fluorophores during polymerization. This did not appear to have any effect on the fluorophores, however it did reduce the background fluorescence of the epoxy.

Initial observations revealed that autofluorescence from 4% paraformaldehyde was sufficient to provide a general tissue label for use with LSCM. This requires relatively high excitation power levels at 488 nm, generally 30–100% of 3.2 mW from a krypton/argon laser, measured at the back focal plane of the objective. The autofluorescent emissions occurred over a range from 500 to over 600 nm and were collected in two different channels as red and green fluorescence. Similarly, autofluorescence could be collected with filters for FITC and Cy3 on an epi-fluorescent microscope. However, significant autofluorescence from the plastic itself is present by epi-fluorescence microscopy, making it difficult to discriminate any but the brightest tissue structures.

Autofluorescence may be collected as a low resolution LSCM image in combination with a specific fluorescent label, such as a cyanine nuclear label, by opening the detector iris and increasing the gain, as shown in Figs. 2C and 3A,B. However, without the use of specific labels, we found it nearly impossible to accurately identify IHCs in degenerating organs of Corti by autofluorescence and nuclear labelling (Fig. 3). Specific labels were also essential in instances where the cochlear duct orientation was not closely aligned to the axis of focus.

Blocks of epoxy-embedded cochlea from archived samples generated for previous studies were examined to assess the usefulness of glutaraldehyde as a protein stain. Glutaraldehyde fluoresces a bright green-yellow when excited at 488 nm. The addition of glutaraldehyde in proportions as low as 0.1% to the paraformaldehyde appeared to significantly increase tissue autofluorescence, to the point of reducing the ability to resolve tissue structures. We found that the presence of 1% osmium tetroxide completely eliminated fixation-induced autofluorescence. Eosin Y was tested for use as a fluorescent nonspecific protein stain. A clearly visible pink color was imparted to the cochlea after only 10 min of incubation in a 0.1% aqueous solution. However, it was weakly fluorescent when imaged by LSCM, and appeared to reduce the fixation-induced autofluorescence. In contrast, eosin Y-stained cochlear tissues were very brightly fluorescent when viewed by epi-fluorescence utilizing the filter set for red fluorescence.

The compatibility of some fluorescent probes with epoxy embedding greatly expanded the utility of this approach by allowing use of lower excitation power levels—3% to 10% of the krypton/argon laser—as well as lower magnifications for some applications (Figs. 2D and 6). Secondary antibodies conjugated to Alexa 488, Alexa 594 and Cy5, and the nucleic acid labels Yo-Pro-1, To-Pro-3 and Neurotrace Red were used successfully. Conjugated fluorescein isothiocyanate (FITC) was found to completely quench upon immersion in unpolymerized Spurr's. Conjugated tetramethyl-
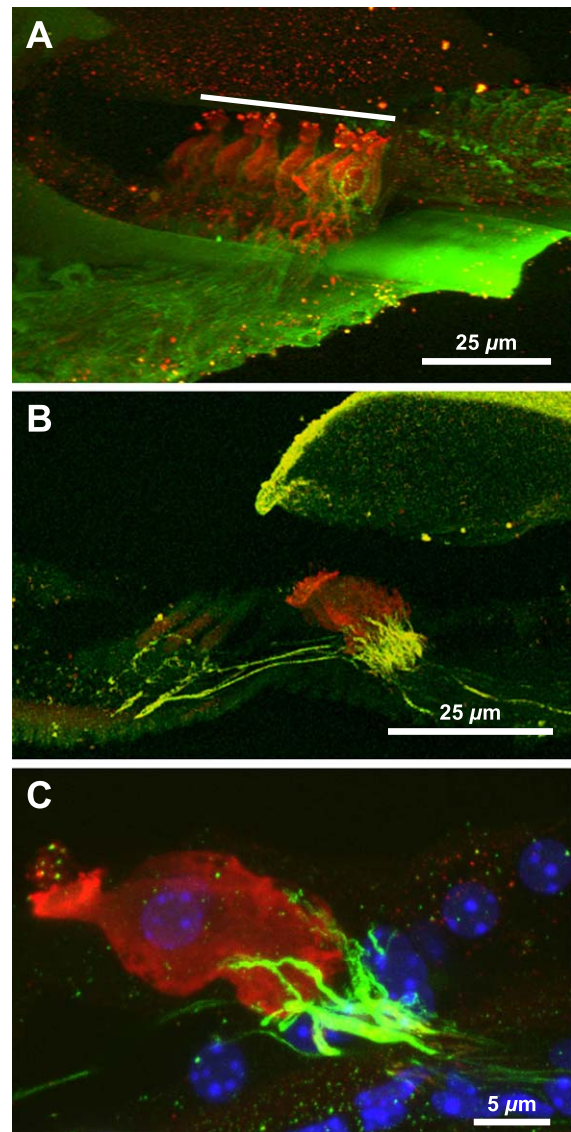
Fig. 4. Pre-embedding immunohistochemistry allows high-resolution views of IHCs and their spatial relationships within the OC. (A) A 60 μm thick optical volume from the lower turn of an aged C57BL/6J mouse was rotated to show an irregular spacing of IHCs resulting from cell loss. The IHCs were labelled for calretinin (red), while beta-tubulin (green) labels nerve fibers, support cells, basal lamina and Hensen's cells. A line drawn over the IHC row shows the length of the cochlear duct in this optical volume (78.2 μm), which appears out of scale due to parallax. LSCM, 60× PlanApo NA 1.4 (Nikon). (B) An optical volume of 38 μm thickness collected by multiphoton LSCM shows the dense arrangement of neurofilaments (green-yellow) innervating the IHC row and calretinin (red) intensely labelling IHCs and weakly labelling OHCs of a young (21 days of age) C57BL/6J mouse. Additional nerve fibers cross the tunnel of Corti, some of which curve upwards to innervate the outer hair cells. 40× PlanNeoFluor NA 1.2 (Zeiss). (C) A high magnification view of two overlapping IHCs in this brightest point projection from the same sample as the previous panel. Calretinin (red) fills the IHC cytoplasm and nerve fibers are heavily labelled for neurofilament (green-yellow). Nuclei labelled with To-Pro-3 (blue) are shown in the proximal IHC and the underlying support cells. LSCM, 60× PlanApo NA 1.4 (Nikon).
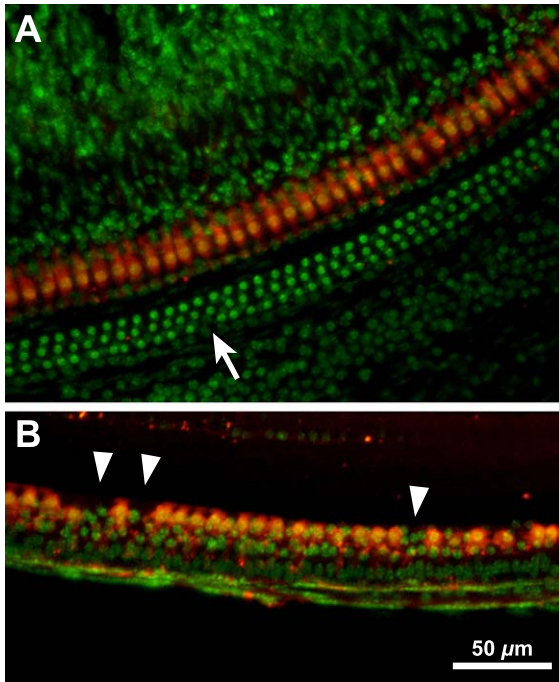
Fig. 5. A surface view at low power illustrates the utility of this protocol for cell counting. IHCs in cochleae from C57BL/6J mice are labelled with calretinin (red) and nuclei are counterstained with Yo-Pro-1 (green). (A) Surface views of young mice with no hearing defects routinely display small numbers of missing outer hair cells (arrow). (B) The upper turn of a 12-month-old C57BL/6J mouse displays moderate IHC loss (arrowheads). LSCM, 20× Fluor NA 0.75 (Nikon).

rhodamine isothiocyanate (TRITC) was partially quenched in unpolymerized Spurr's and completely quenched after polymerization.

While the probes for DNA and RNA required only 45 min of incubation for labelling the organ of Corti, the minimum incubation period for consistent immunohistochemical labelling was found to be 3 days for primary antibodies and 2 days for secondary antibodies. These times generally gave complete labelling through the cochlear duct. Attempts to label the spiral ganglion were partially successful with the nucleic acid probes and some antibody labels. Fluorescent label was generally observed to penetrate the habenulae perforata and fade towards the center of the modiolus.

A variety of specific antibodies allowed ready identification of the IHCs, neural processes and support cells. OHCs could be identified by nuclear label alone in relatively intact organs, with favorable orientation (Figs. 2D, 3A, 4B, 5A,B, 6A and 7A–C). However, in age-degenerated or otherwise unfavorable specimens (Figs. 3B–D and 4A, for example) OHCs could only be identified with certainty with the use of specific labels, such as a monoclonal antibody against prestin (results not shown).

Multi-photon LSCM imaging (Fig. 4B) provided optical volumes with less light attenuation through the volume than experienced with conventional LSCM. However, laser power at or above 10% was found to cause melting of the epoxy

resin with production of small pits of burned plastic in the block face.

Cell counting in optical volumes was readily accomplished using Object Image. A 3D object defined for length was used to measure the length of the basal lamina while stepping through the z-stack. An example of such a measure may be seen in Fig. 4A. This z-series stack was obtained by focusing 60 μm through the surface of a slab in a modiolar
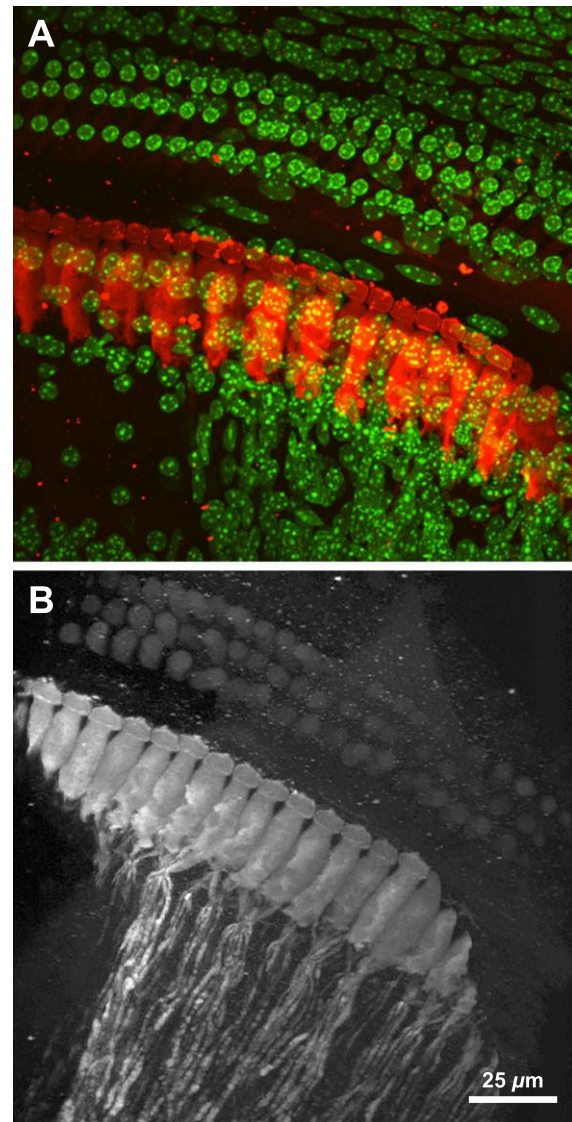
Fig. 6. Two surface views from the cochlea of a 21-day-old C57BL/6J mouse show differences in the packing of IHC cell bodies along the cochlear duct. (A) The upper turn viewed from the direction of the tectorial membrane shows IHCs labelled by calretinin (red) while the three rows of OHCs are identified by nuclear label (green). The IHC cell bodies are seen to be overlapping one another, with alternate cells lying in 2 different planes, while their cuticular plates maintain a stereotypical regular arrangement. (B) A single channel projection viewed from the direction of the inner pillar cells in the lower turn reveals that the somata of calretinin labelled IHCs appear tightly packed in a single plane. Nerve fiber bundles are observed to constrict as they pass through the habenula perforata then spread out to innervate the IHCs. LSCM, 60× PlanApo NA 1.4 (Nikon).

view orientation, at increments of 0.4 μm. The measured length of the cochlear duct often did not equal the thickness of the optical volume, due to the angle of the cochlear duct relative to the plane of focus. In the instance shown in Fig. 4A, the angle was approximately 40° in the Y-axis. A
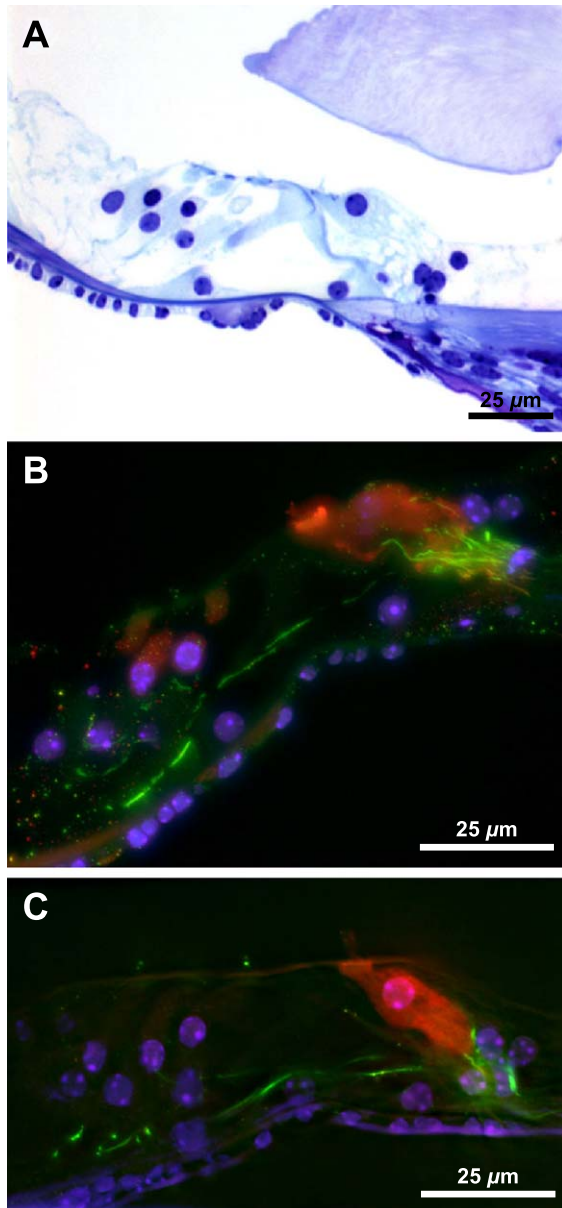
Fig. 7. Epi-fluorescence microscopy on an embedded cochlea from a 21-day-old C57BL/6J mouse previously imaged by LSCM. (A) Toluidine blue staining of a 3 μm thick section from a sample previously labeled for calretinin and DNA. (B) Conventional epi-fluorescence image of a 3 μm section presents an IHC labelled for calretinin (red), neurofilament (green) and nuclei (blue). Some nerve fibers form synapses on the IHC, while others are crossing the tunnel of Corti and branching upwards toward the outer hair cells. This image is a brightest point projection from seven levels through a 3 μm section. (C) A 20 μm thick optical volume collected from the same block from which the section in (B) was cut. This z-series was deconvolved by the nearest neighbors method. 40× PlanFluor NA 0.75 (Zeiss).

second 3D object, defined for points, recorded IHC nuclei as they came into view while stepping through the z-stack.

Image processing software allowed rotation of optical volumes about their X- or Y-axes to correct for misalignments due to the angle and curvature of the cochlear duct relative to the focal axis. Two-dimensional images created from brightest point projections in the Z-axis allowed superimposition of structural elements from multiple optical sections to create composite views showing a great degree of detail (Figs. 2C, 4C, 6A,B and 7C). Brightest point projection rotations were also employed to realign the optical volume to specific viewpoints (Figs. 3C,D, 4A,B, 5A,B and 6A,B). Rotating projections were particularly useful to impart a sense of depth and 3D spatial relationships.

Modiolar views of labelled cochlea were collected by epi-fluorescence microscopy in a manner similar to that described for confocal microscopy. Volumes were collected 20–80 μm deep into the sample. Deconvolution by a nearest neighbors algorithm, using a calculated point spread function, was applied to the optical volume to create very sharp, high-resolution images (Fig. 7C). Conventional semi-thin sections, 1–3 μm, cut from the samples before or after imaging were attached to slides and either stained with a conventional histological stain (Fig. 7A), or mounted with a coverslip and imaged by epi-fluorescence microscopy (Fig. 7B).

Additional videos and 3D images of material imaged in this project: http://depts.washington.edu/rubelab/.

7. Discussion

This paper describes a new method for microscopy and 3D reconstruction of the mammalian cochlea offering several advantages over alternative histological preparations. The surface preparation, for example, is very useful in allowing gross and cellular morphometry over large regions of the cochlear duct [2]. However, this technique requires considerable dissection skills and is susceptible to distortion and sample losses. Embedding the surface preparation in plastic [1,7] provides improved ease of preparation and durability of the sample, and results in greater clarity and resolution by brightfield microscopy. However, the method's reliance on brightfield microscopy through thick samples limits its specificity and resolution and often necessitates subsequent sectioning for brightfield or electron microscopy. A three-dimensional reconstruction from such sections requires realignment of large numbers of sections and manual tracings of features of interest. Such efforts limit these studies to those features that may be traced over small volumes, or a small number of cells [4–6]. In vitro imaging using multiple fluorescent probes provides greater differentiation of cell and tissue types within the organ of Corti [3], and allows direct capture of optical volumes through the organ of Corti for reorientation using imaging software. However, in vitro imaging is technically challenging and not

readily available to many labs, and is incompatible with most antibody labelling, relying instead on vital dyes. Our method combines the specificity of fluorescent probes with the clarity and durability of epoxy embedding to allow fluorescent microscopy of the cochlea at gross, cellular and subcellular levels of resolution for the generation of conventional images and 3D optical volumes. Furthermore, the samples are relatively easily prepared and readily imaged by a variety of approaches.

The primary issues associated with the fluorescent labelling of epoxy-embedded cochleae were (a) the compatibility of the fluorophore with the plastic, and (b) penetration of the antibodies into the cochlear duct.

We found that FITC and TRITC failed to fluoresce after embedding, as viewed by epi-fluorescence and LSCM. This may be a result of environmental conditions within the resin, such as pH, to which these dyes are known to be susceptible [9]. The absorption curve of eosin Y (2′,4′,5′,7′-tetrabromo-fluorescein) has a sharply defined, narrow peak centered at 525 nm. This peak lies between the 488 and 568 nm laser lines used on our LSCM, which would have been weakly absorbed by this fluorophore, resulting in a corresponding weak fluorescent emission. On the other hand, eosin Y appeared to quench autofluorescence in the embedded cochlea. Its constituent bromines are known to cause quenching by promoting intersystem crossing, a mechanism of energy loss whereby an excited fluorophore returns to ground state without emission of a photon [9]. Additionally, eosin Y is known to produce high levels of singlet oxygen upon light absorption, which can also lead to quenching of adjacent fluorophores [9]. However, eosin Y was brightly fluorescent by epi-fluorescence. It may be useful as a generalized fluorescent protein stain for imaging the cochlea by epi-fluorescence or by LSCM with appropriate laser lines.

Antibody penetration may be assessed by comparing the intensity of labelling across the different cochlear turns, or by noting the degree of penetration of label into the spiral ganglion following varying incubation periods. Some primary antibodies gave much more variable degrees of labelling than did others. Such variations may be the result of differences in avidity or in the perfusion of antibodies through the cochlear labyrinth. Antibodies with higher avidity may give increased labelling over shorter periods of contact with their epitopes, making variability in circulation of the reagent less significant. Antibody infiltration might be facilitated by making small holes in the otic capsule along the cochlear spiral. Non-immunologic labels such as the monomeric cyanine nuclear labels and the fluorescent Nissl stains (not shown) are able to quickly penetrate the sample, including the modiolus and spiral ganglion. This is most likely due to the small size of these fluorophores (<1000 Da) relative to antibodies (150,000 Da). Further work will be required to determine if increased incubation times can overcome the problem of penetrating the tissues of the modiolus with antibodies or whether the structure will require specific chemical or mechanical per-

meabilization. It also remains to be seen whether prolonged washes after incubations with primary and secondary antibodies are of value in reducing the punctate background label sometimes observed within the organ of Corti.

Imaging by LSCM with a combination of autofluorescence and nuclear labelling provided sufficient resolution in the intact, well organized organ of Corti such that inner hair cells could be counted using a $60\times$ objective. However, in aged cochleae displaying significant hair cell loss, even a threefold zoom of the image from a $60\times$ objective was not sufficient to enable IHCs to be distinguished from surviving support cells with certainty. Application of specific markers allowed hair cells to be readily identified in the degenerating organ of Corti with a $60\times$ objective without zoom. Even a $20\times$ objective, with optional use of zoom, could be used to identify IHCs labelled for calretinin in the normal and damaged organ of Corti.

The power of the exciting laser beam attenuated as it was focused through the epoxy. Although increasing excitation power levels up to 30% allowed imaging 180–200 μm into the epoxy with a $60\times$ objective, the fluorescent labelled structures near the sample surface had saturated intensities with this laser intensity. High power levels also led to more rapid photo-bleaching. This approach may be useful for some studies, such as counting cells without regard to internal structural information. We restricted our sample volumes to a depth of 60 μm to allow reduced laser power levels while still yielding sufficient image volume for cell counting and 3D reconstructions.

The multi-photon LSCM provided images with less attenuation through optical volumes of 60–80 μm. However, utility of multi-photon imaging may be limited by the susceptibility of the epoxy to heating damage from high laser intensities. Deeply imaging into the block with reduced laser power prevented heating effects, but the prolonged scanning appeared to cause photo-bleaching.

A well-oriented surface view allows long portions of the organ of Corti to be reviewed with a low magnification objective. Surface view preparations require careful alignment of the saw blade parallel to the basal lamina to minimize the risk of sawing through the organ of Corti. Conversely, failure to remove enough of the overlying plastic will result in long working distances that may prevent focusing on the cells of interest.

Although conventional epi-fluorescence microscopy is useful for approximately orienting the samples for LSCM, the confocal is significantly more efficient for reviewing tissue morphology. The high degree of light scattering and autofluorescence from both tissue and plastic in these samples gave an extremely blurry image when viewed by conventional epi-fluorescence. However, deconvolution by nearest neighbours and constrained interactive algorithms produced very clear images from sample volumes collected at depths up to 80 μm.

Single sections cut from these blocks and viewed by epi-fluorescence presented high-resolution images of fluores-

cently labelled cochlear structures. These semi-thin sections may also be stained with conventional histological stains, allowing traditional section-based histological analyses. This approach for labelling sections has two distinct advantages over traditional immunofluorescent methods for plastic sections: there is no need for etching of the plastic by harsh agents, such as sodium ethoxide, which may destroy antigens; in addition, the label extends through the depth of the section rather than being restricted to those epitopes exposed on the etched surface of the plastic section.

Additional refinements to this method will further improve its applicability to future cochlear studies, as well as to other fields. Advances in improving penetration of antibodies and other probes into the deeper tissues, such as the spiral ganglion, will add to the range of applications for this method.

8. Quick procedure

1. Dissect, fix and decalcify cochleas.
2. Perform immunohistochemical labelling of cochleas.
3. Dehydrate and embed cochleas in resin.
4. Orient and polymerize cochleas in molds.
5. Cut slabs of tissue using a diamond wheel saw and affix to blank blocks of resin.
6. Image tissue using confocal microscope.

Acknowledgements

References

[1] B.A. Bohne, Location of small cochlear lesions by phase contrast microscopy prior to thin sectioning, Laryngoscope 82 (1972) 1–16.

[2] H. Engstrom, H.W. Ades, A. Andersson, Structural Pattern of the Organ of Corti. Systematic Mapping of Sensory Cells and Neural Elements, Almqvist & Wiksell, Stockholm, 1966, 172 pp.

[3] Å. Flock, E. Scarfone, M. Ulfendahl, Vital staining of the hearing organ: visualization of cellular structure with confocal microscopy, Neuroscience 83 (1998) 215–228.

[4] S. Hashimoto, R.S. Kimura, T. Takasaka, Computer-aided three-dimensional reconstruction of the inner hair cells and their nerve endings in the guinea pig cochlea, Acta Oto-Laryngol. 109 (1990) 228–234.

[5] M.C. Liberman, L.W. Dodds, S. Pierce, Afferent and efferent innervation of the cat cochlea: quantitative analysis with light and electron microscopy, J. Comp. Neurol. 301 (1990) 443–460.

[6] M. Sato, M.M. Henson, O.W. Henson Jr., D.W. Smith, The innervation of outer hair cells: 3D reconstruction from TEM serial sections in the Japanese macaque, Hear. Res. 135 (1999) 29–38.

[7] H. Spoendlin, J.-P. Brun, The block-surface technique for evaluation of cochlear pathology, Arch. Oto-Rhino-Laryngol. 208 (1974) 137–145.

[8] X.J. Sun, L.P. Tolbert, J.G. Hildebrand, Using laser scanning confocal microscopy as a guide for electron microscopic study: a simple method for correlation of light and electron microscopy, J. Histochem. Cytochem. 43 (1995) 329–335.

[9] N.J. Turro, Molecular Photochemistry, W.A. Benjamin, New York, 1965, 286 pp.